Dissolution and Stabilization of Platinum in Oxygen Cathodes

Kotaro Sasaki, Minhua Shao, and Radoslav Adzic

Abstract In this brief review of the dissolution and solubility of platinum under equilibrium conditions and the degradation of platinum nanoparticles at the cathode under various operating conditions, we discuss some mechanisms of degradation, and then offer recent possibilities for overcoming the problem. The data indicate that platinum nanoparticle electrocatalysts at the cathode are unstable under harsh operating conditions, and, as yet, often would be unsatisfactory for usage as the cathode material for fuel cells. Carbon corrosion, particularly under start/stop circumstances in automobiles, also entails electrical isolation and aggregation of platinum nanoparticles. We also discuss new approaches to alleviate the problem of stability of cathode electrocatalysts. One involves a class of platinum monolayer electrocatalysts that, with adequate support and surface segregation, demonstrated enhanced catalytic activity and good stability in a long-term durability test. The other approach rests on the stabilization effects of gold clusters. This effect is likely to be applicable to various platinum- and platinum-alloy-based electrocatalysts, causing their improved stability against platinum dissolution under potential cycling regimes.

1 Introduction

One critical issue facing the commercialization of low-temperature fuel cells is the gradual decline in performance during operation, mainly caused by the loss of the electrochemical surface area (ECA) of carbon-supported platinum nanoparticles at the cathode. The major reasons for the degradation of the cathodic catalyst layer are the dissolution of platinum and the corrosion of carbon under certain operating conditions, especially those of potential cycling. Cycling places various loads on

K. Sasaki, M. Shao, and R. Adzic (✉)
Department of Chemistry, Building 555, Brookhaven National Laboratory,
P.O. Box 5000, Upton, NY 11973-5000, USA
e-mail: ksasaki@bnl.gov, adzic@bnl.gov

fuel cells; in particular, stop-and-go driving, and fuel starvation in vehicular applications can generate high voltage loads. The coalescence of platinum nanoparticles through migration also results in the loss of surface area. Hence, a detailed understanding of degradation mechanisms of platinum nanoparticles will help in designing durable materials for the oxygen reduction reaction (ORR).

In this review, we briefly discuss the dissolution and solubility of platinum (Sect. 2), the degradation of platinum nanoparticles in fuel cells (Sect. 3), and carbon corrosion (Sect. 4). We then describe new cathode electrocatalysts wherein the platinum content can be dramatically reduced, while offering possibilities for enhancing catalytic activity and stability (Sect. 5).
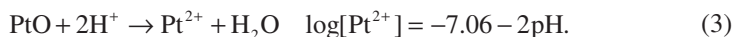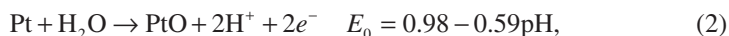
2 Platinum Dissolution

2.1 Bulk Material

The thermodynamic behavior of a platinum bulk material as a function of electrolyte pH and electrode potential is guided by potential–pH diagrams (also known as Pourbaix diagrams) (Pourbaix 1974). The main pathways for platinum dissolution at 25°C involve either direct dissolution of metal,
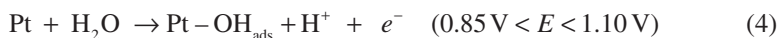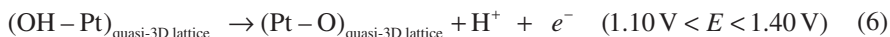
$$Pt \rightarrow Pt^{2+} + 2e^- \quad E_0 = 1.19 + 0.029\log[Pt^+], \tag{1}$$
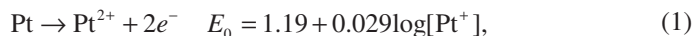
or production of an oxide film and a subsequent chemical reaction,

$$Pt + H_2O \rightarrow PtO + 2H^+ + 2e^- \quad E_0 = 0.98 - 0.59pH, \tag{2}$$

$$PtO + 2H^+ \rightarrow Pt^{2+} + H_2O \quad \log[Pt^{2+}] = -7.06 - 2pH. \tag{3}$$

The potential–pH diagram suggests that platinum is fairly stable thermodynamically; there is only a small corrosion region around 1 V at pH −2 to 0 (we note that the potential–pH diagram is valid only in the absence of ligands with which platinum can form soluble complexes or insoluble compounds). However, as described below, platinum actually dissolves under fuel cell operating conditions, which is unsatisfactory especially for its usage in the cathode of fuel cells for automotives.

Conway et al. (Angerstein-Kozlowska et al. 1973; Conway 1995) summarized earlier work on platinum oxide formation; in the potential region of 0.85–1.10 V in an H_2SO_4 solution, adsorbed species (OH_{ads}) are formed by the oxidation of H_2O molecules (4). The OH_{ads} and platinum surface atoms then undergo place-exchange, forming a quasi-3D lattice (5). At higher potentials (1.10–1.40 V), the OH species in this lattice are oxidized, generating a Pt–O quasi-3D lattice (6).

$$Pt + H_2O \rightarrow Pt - OH_{ads} + H^+ + e^- \quad (0.85\,V < E < 1.10\,V) \tag{4}$$

$$Pt-OH_{ads} \xrightarrow{\text{place exchange}} (OH-Pt)_{\text{quasi-3D lattice}} \qquad (5)$$

$$(OH-Pt)_{\text{quasi-3D lattice}} \rightarrow (Pt-O)_{\text{quasi-3D lattice}} + H^+ + e^- \quad (1.10\,V < E < 1.40\,V) \quad (6)$$

However, recent studies using an electrochemical quartz crystal nanobalance revealed that the platinum oxides are not hydrated (Birss et al. 1993; Harrington 1997; Jerkiewicz et al. 2004); thus, at 0.85–1.15 V a half monolayer (0.5 ML) forms from chemisorbed oxygen (O_{chem}), rather than $OH_{ads.}$. Figure 1 depicts the proposed mechanism. First, H_2O molecules adsorb on the platinum electrode at low potentials (0.27–0.85 V) since the platinum surface partial positive charge can be compensated for by the negatively charged oxygen end of the H_2O molecule (Fig. 1a). At potentials between 0.85 and 1.15 V, the discharge of 0.5 ML of H_2O molecules occurs, thereby leading to the formation of 0.5 ML of O_{chem} (Fig. 1b). Above a potential of 1.15 V, further discharge of H_2O results in the formation of the second 0.5 ML of O_{chem}, with the first 0.5 ML O_{chem} (Fig. 1c). During this process, strong dipole–dipole lateral repulsions cause the initial 0.5 ML O_{chem} adatoms to undergo place-exchange with platinum atoms, so forming a quasi-3D surface Pt–O lattice (Fig. 1d). You et al.
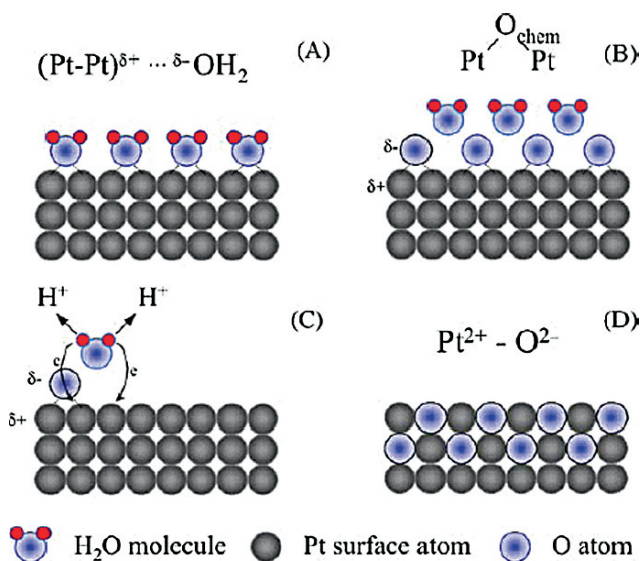

Fig. 1 The PtO growth mechanism (Jerkiewicz et al. 2004). (**a**) Interactions of H_2O molecules with the platinum surface that occur in the $0.27 \leq E \leq 0.85\,V$ range. (**b**) Discharge of a half monolayer of H_2O molecules and subsequent formation of a half monolayer of chemisorbed oxygen (O_{chem}) in the $0.85 \leq E \leq 1.15\,V$ range. (**c**) Discharge of the second half monolayer of H_2O molecules at $E > 1.15\,V$; the process is accompanied by the development of repulsive interactions between $(Pt-Pt)^{\delta+}-O^{\delta-}_{chem}$ surface species that stimulate an interfacial place-exchange of O_{chem} and platinum surface atoms. (**d**) Formation of a quasi-3D surface PtO lattice comprising Pt^{2+} and O^{2-} moieties through the place-exchange process

found that only 0.3 ML of platinum atoms exchange places with the oxygen-containing species (You et al. 2000; Nagy and You 2002). This mechanism exposes platinum to the electrolyte, thereby promoting its oxidation and dissolution (Wang et al. 2006b). Nagy and You (Nagy et al. 2002) demonstrated that PtO is mobile and can diffuse to energetically favorable sites on the platinum surface, so increasing the exposure of the underlying platinum atoms to the electrolyte. At higher potentials, more of the PtO film is oxidized to PtO_2, which also is mobile (You et al. 2000).

2.2   Equilibrium Solubility of Platinum

The solubility of platinum changes with various factors, including potentials, electrolyte components, pH, and temperature. Azaroual et al. (2001) examined the solubility of platinum wires and particles in several buffer solutions of pH 4–10 at 25°C. They found that the solubility of platinum increases with increasing pH, suggesting that the hydroxylated complex $PtOH^+$ is a major determinant of platinum solubility in this pH range. They also reported that the solubility of platinum particles (diameter 0.27–0.47 μm) is two orders of magnitude higher than that of platinum wires. By contrast, platinum solubility increases with decreasing pH in sulfuric acid (pH < 1.5); apparently, dissolution of platinum in the acidic medium follows an acidic dissolution mechanism (Mitsushima et al. 2007b). Platinum solubility strongly depends on the temperature (Dam and de Bruijn 2007), rising with increasing temperature, following the Arrhenius relationship (Mitsushima et al. 2007a, b).

There are extensive studies of the effect of potential on platinum solubility in acidic solutions (Bindra et al. 1979; Ferreira et al. 2005; Wang et al. 2006a, b Dam et al. 2007 ; Mitsushima et al. 2007a, b). Figure 2 shows a plot of the published data on dissolved platinum concentrations as a function of applied potential, summarized by Mitsushima et al. (2007a, b), Borup et al. (2007), and Shao-Horn et al. (2007). We also include those data calculated from (1), i.e., the two-electron dissolution process, as we indicate by the Pourbaix's diagram at two different temperatures (dashed-dotted line at 25°C, and solid line at 196°C). Overall, the equilibrium concentration of dissolved platinum increases with increasing potentials up to 1.1 V. The solubility data in a concentrated H_3PO_4 solution (18.6 M) at 196°C obtained by Bindra et al. (1979) (open circles in Fig. 2) agree well with those calculated from (1) at the same temperature, suggesting that platinum dissolution underwent a two-electron reaction pathway in the experiment. Except for this case, however, the slopes of all other experimental data are much less than those calculated from the Pourbaix diagram. Although the origin of the discrepancy between the solubility data and the Pourbaix model is unclear, platinum dissolution might involve chemical processes, such as the dissolution of PtO in other electrochemical reactions (Mitsushima et al. 2007a, b). Another notable feature in Fig. 2 is that the solubility of platinum wire in 0.57 M $HClO_4$ at 23°C starts to decline at potentials over 1.1 V. As we described in Sect. 2.1, above 1.15 V the place-exchange process starts and a 3D PtO film is formed; accordingly, this retardation in platinum solubility can be attributed to the formation of a protective overlying oxide film (Mitsushima et al. 2007a, b).
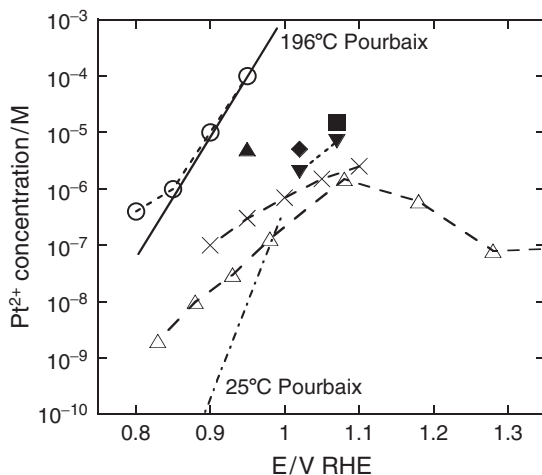
Fig. 2 Dissolved platinum concentrations as a function of potential. *Crosses* 76°C in 1 M H_2SO_4 (Ferreira et al. 2005), *open triangles* 23°C in 0.57 M $HClO_4$ (Wang et al. 2006), *circles* 196°C in concentrated H_3PO_4 (Bindra et al. 1979), *inverted filled triangles* 23°C in 1 M H_2SO_4, *upright filled triangle* 35°C in 1 M H_2SO_4, *square* 51°C in 1 M H_2SO_4, *diamond* 76°C in 1 M H_2SO_4 (Mitsushima et al. 2007). The *dashed-dotted lines* and the *solid lines* were calculated from the Pourbaix diagram at 25°C and 196°C, respectively. *RHE* reversible hydrogen electrode

Platinum dissolution also depends on crystallographic orientation. Komanicky et al. (2006) studied the dissolution on different low-index facets in 0.6 M $HClO_4$ solution at three different potentials (0.65, 0.95, 1.15 V). Even at the low 0.65-V potential, they observed dissolution at edges and pits on the Pt(111) surface, while the terrace was stable. Surprisingly, dissolution was inhibited at 0.95 V owing to the formation of oxide films at the edges, but it started again at 1.15 V, when the terrace plane was irreversibly roughened with multiple pits on its surface. For Pt(100) and (110) facets, dissolution declined with increasing potential owing to the formation of a passive layer on their surfaces. These authors also explored the changes on a nanofaceted platinum surface consisting of alternating (111) rows and (100) facets of several nanometer width, to simulate the behavior of platinum nanoparticles. They reported that the extent of the nanofaceted surface that dissolved rose with increasing potentials and almost entire nanofacets had been dispersed at 1.15 V, suggesting that the edges and corners on platinum nanoparticles, with their low coordinate sites, might have a higher tendency to dissolve away compared with the terraced facets.

2.3 Dissolution Under Potential Cycling

Potential cycling conditions accelerate platinum dissolution compared with potentiostatic conditions (Johnson et al. 1970; Rand and Woods 1972; Kinoshita et al. 1973; Ota et al. 1988). For example, Wang et al. (2006a, b) reported that the dissolution rates under potential cycling are 3–4 orders of magnitude higher than

those determined for potentiostatic conditions. The dissolution rate during triangular potential cycling reportedly was around 2–5.5 ng cm^{-2} per cycle, with the upper potential limit between 1.2 and 1.5 V and various potential scanning rates (Johnson et al. 1970; Rand et al. 1972; Kinoshita et al. 1973; Wang et al. 2006a, b). The dissolution rate increased with a rise in the upper potential limit (Rand et al. 1972). Meyers and Darling (Darling and Meyers 2003, 2005) developed a mathematical model based on the reactions in (1)–(3) to study the dissolution and movement of platinum in a proton exchange membrane fuel cell (PEMFC) during potential cycling from 0.87 to 1.2 V. The oxide film that developed was found to retard dissolution markedly. Dissolution was severe when the potential switched to an upper limit of 1.2 V, but then it stopped once a monolayer of PtO had accumulated. However, we lack detailed knowledge of mechanisms of dissolution, and of the particular species dissolved during potential cycling.

Rand and Woods (1972) detected both Pt(II) and Pt(IV) ions after 200 triangular potential cycles between 0.41 and 1.46 V at 40 mV s^{-1} in 1 M H$_2$SO$_4$. They found that the charge difference between anodic and cathodic cycles in oxygen adsorption and desorption regions ($Q_o^a - Q_o^c$) was positive and consistent with the amount of platinum dissolved. Therefore, they considered that anodic dissolution during anodic scans, partly either via the reaction in 1 or via that in (2) and (3), is the main cause.

On the other hand, a "cathodic" dissolution mechanism has been suggested; Johnson et al. (1970) detected Pt(II) in a rotating ring-disk electrode study during the negative-going potential scan in a 0.1 M HClO$_4$ solution. The Pt(II) species formed due to the reduction of PtO$_2$ (Johnson et al. 1970; Mitsushima et al. 2007a):

$$PtO_2 + 4H^+ + 2e^- \rightarrow Pt^{2+} + 2H_2O \quad E_0 = 0.84 + 0.12 pH + \log[Pt^{2+}]. \qquad (7)$$

In this case, the charge difference between the anodic and cathodic scans $Q_o^a - Q_o^c$ is also positive because the charge is less than that needed to reduce adsorbed oxygen to water since only one electron is used for each oxygen atom (Rand and Woods 1972). Mitsushima et al. (2007a, b) compared the dissolution rates of platinum in sulfuric acid during potential cycling with four different potential profiles. Among them, the slow cathodic triangular sweep (20 mV s^{-1} anodic and 0.5 mV s^{-1} cathodic) showed a significantly enhanced dissolution rate, attaining over 20 ng cm^{-2} per cycle and an electron transfer number of 2 [indicating that the dissolved species is Pt(II)]; at the other potential-wave modes the dissolution rate remained around a few nanograms per square centimeter per cycle with an electron transfer number of 4, indicating that the dissolved species is Pt(IV). The enhanced platinum dissolution during the slow cathodic scans is considered to follow the cathodic-dissolution mechanism represented in (7).

3   Degradation of Platinum Nanoparticles in Fuel Cells

Extensive studies on catalyst degradation in PEMFCs and phosphoric acid fuel cells (PAFCs) demonstrated that its cause can be attributed mainly to a loss of ECA in the cathode. PEMFCs and PAFCs use similar catalysts, although the degradation

in PAFCs generally is severer because of the relatively higher cell temperature (200°C) at which they operate, and the use of a more corrosive electrolyte. Shao-Horn et al. (2007) proposed classification of four mechanisms for the decrease in ECA (1) crystallite migration on carbon supports forming larger particles, (2) platinum dissolution and its redeposition on larger particles (electrochemical Ostwald ripening), (3) platinum dissolution and precipitation in ion conductors, and (4) the detachment and agglomeration of platinum particles caused by carbon corrosion. The fourth mechanism is discussed in Sect. 4.

3.1 Crystallite Migration and Coalescence

This mechanism involves the migration of platinum nanoparticles on the carbon support and their coalescence during fuel cell operations (Fig. 3a); no platinum dissolution is involved. The underlying driving force minimizes the total surface energy as the surface energy of the nanosized particles declines with the particles' growth. This mechanism of particle growth generates a specific particle size distribution, which peaks at small sizes, tailing toward larger sizes. In fact, it was observed in both PAFC (Bett et al. 1976; Blurton et al. 1978; Aragane et al. 1988) and PEMFC (Wilson et al. 1993) studies. Wilson et al. recorded such a size distribution of aged platinum nanoparticles in the cathode by X-ray diffraction analysis. They suggested that particle growth in PEMFCs is caused by the crystalline migration mechanism, not by a dissolution–redeposition process that results in a different size distribution, as we discuss below (Wilson et al. 1993). Other evidence supporting the particle-migration mechanism arises from the demonstrated insensitivity of ECA loss during the operation of PAFCs to the potential (Blurton et al. 1978; Gruver et al. 1980),
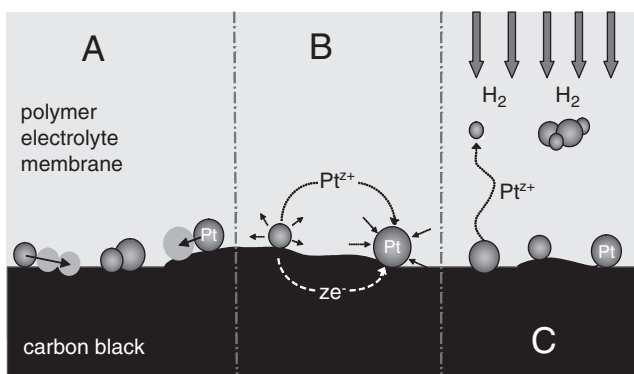

Fig. 3 Three mechanisms for the degradation of carbon-supported platinum nanoparticles in low-temperature fuel cells. (**a**) Particle migration and coalescence. (**b**) Dissolution of platinum from smaller particles and its redeposition on larger particles (electrochemical Ostwald ripening). (**c**) Dissolution of platinum and its precipitation in a membrane by hydrogen molecules from the anode

suggesting that dissolution–redeposition is not the dominant mechanism. We note that most of the data supporting the migration mechanism were obtained below 0.8 V, at which point the solubility of platinum is low, and, therefore, platinum dissolution is not considered dominant at these relatively lower potentials.

3.2   Dissolution and Redeposition: Electrochemical Ostwald Ripening

The second mechanism involves the dissolution and redeposition of platinum on large particles. If platinum is partially soluble in electrolytes/ionomers, smaller particles will dissolve preferentially as their chemical potential is higher than that of larger platinum particles (Voorhees 1985; Virkar and Zhou 2007). Dissolved platinum species move to the surfaces of larger particles through the electrolyte/ionomer, while electrons are transported through the carbon supports to larger particles. Thus, platinum is precipitated at the surfaces of larger particles. As particle size falls, the chemical potential increases, and so dissolution accelerates, resulting in the growth of large particles at the expense of small ones with the necessary concomitant decrease in the system's total energy. Honji et al. (1988) recorded potential-dependent particle growth at 205°C in PAFCs. They showed that the platinum particle's size starts to increase and the amount of platinum in the electrode decreases above 0.8 V, suggesting that platinum dissolution and redeposition is the main mechanism for particle growth at high potentials (Tseung and Dhara 1975; Honji et al. 1988). Their notion is supported by Bindra et al.'s (1979) experiment that demonstrated an exponential increase in the solubility of a platinum foil in phosphoric acid at 176–196°C above 0.8 V. Virkar and Zhou (2007) found that electronically conductive supports, such as carbon black, are critical for this process. Platinum particles did not grow when they were supported on nonconductive Al_2O_3 because this growth process involves a coupled transport of platinum ions and electron transport via water/ionomer and conductive supports. The dissolution–redeposition of platinum on carbon supports is considered an analogy of the Ostwald ripening mechanism (Voorhees 1985); however, this mechanism apparently accompanies the electrochemical reactions, and thus is sometimes termed "electrochemical Ostwald ripening" (Honji et al. 1988).

It is difficult to rationalize the contributions of crystallite migration and coalescence and of Oswald ripening to the ECA loss in PEMFCs. The size distributions of platinum particles are sometimes employed to differentiate them, as the electrochemical Ostwald ripening process is characterized by an asymmetric particle distribution with a tail toward the small particle end owing to the consumption of smaller particles (Wilson et al. 1993), while crystallite migration and coalescence has a tail toward large particles, as we described in Sect. 3.2. However, some researchers observed a bimodal distribution of particle size during potential cycling (Xie et al. 2005a; Garzon et al. 2006), suggesting that a combination of these two processes takes place (Bindra et al. 1979).

3.3   Platinum Dissolution and Precipitation in Membranes

The third mechanism also involves the dissolution of platinum; however, thereafter, the dissolved platinum species diffuse into a membrane and are reduced chemically by hydrogen permeating from the anode (Fig. 3c). The direct evidence supporting this mechanism is the observation of platinum particles in the matrix (Aragane et al. 1988) and membrane (Patterson 2002) after fuel cell operation. The driving force underlying the crossover of dissolved platinum species into the membrane could be electro-osmotic drag and/or the concentration gradient diffusion (Guilminot et al. 2007a, b). The particular counteranions of Pt^{z+} have not yet been established. Membrane degradation products, such as fluoride (Healy et al. 2005; Xie et al. 2005b) and sulfate (Xie et al. 2005a, b; Teranishi et al. 2006) anions were detected during the operation of PEMFCs, and could possibly be the complexing ligands for Pt^{z+}. In fact, strong evidence from Guilminot et al. (2007b) demonstrated that the concentration of fluoride around the platinum nanoparticles in an aged membrane was higher than that in a new membrane. Another possible source is other halide ions, such as chloride and bromide, left on carbon and platinum surfaces during the synthesis of the catalyst (Guilminot et al. 2007a, b). Both mobile Pt(II) and Pt(IV) species were detected in the fresh/aged membrane electrode assemblies. The concentrations of these species increase upon ageing, and these ions are highly mobile in the membrane (Guilminot et al. 2007a, b). The platinum band or large particles form in the membrane near the interface of the membrane/cathode during cycling with H_2/N_2 (Ferreira et al. 2005; Yasuda et al. 2006a, b; Ferreira and Shao-Horn 2007) and somewhere away from the cathode with H_2/O_2(air) (Patterson 2002; Yasuda et al. 2006a, b; Bi et al. 2007; Zhang et al. 2007a). Platinum can move into the anode with absence of H_2 (Yasuda et al. 2006a, b). These results strongly point to the chemical reduction by H_2 of Pt^{z+} in the membrane. Some studies combining experimental data and mathematical models revealed that the location of the platinum band in the membrane under open circuit voltage (OCV) and cycling conditions depends on the partial pressure of H_2 and O_2 and also their permeability and that of Pt^{z+} through the membrane (Bi et al. 2007; Zhang et al. 2007a, b).
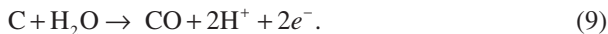
4   Carbon Corrosion

4.1   General Aspects of Carbon Corrosion

Corrosion of carbon supports may cause the electrical isolation and aggregation of platinum nanoparticles, causing a decrease in the ECA in the catalyst layers too. The electrochemical behaviors of carbon in different forms have been studied under a variety of conditions; there is a comprehensive review of works conducted two decades ago in Kinoshita's classic book (Kinoshita 1988). In aqueous solutions, the general carbon corrosion reaction can be written as (Kinoshita 1988)

$$C + 2H_2O \rightarrow CO_2 + 4H^+ + 4e^-, \tag{8}$$
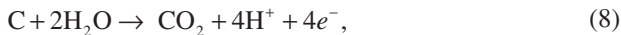
with a standard potential of 0.207 V versus the standard hydrogen electrode, indicating that carbon can be thermodynamically oxidized at potentials above 0.207 V. To a lesser extent, the heterogeneous water–gas reaction (Stevens et al. 2005) also can occur with a standard potential of 0.518 V:

$$C + H_2O \rightarrow CO + 2H^+ + 2e^-. \tag{9}$$

However, the corrosion rate of carbon at potentials lower than 0.9 V is reasonably slow at the typical operating temperatures (60–90°C) of PEMFCs. Despite the sluggishness of the reaction, long-term operations can cause a decrease in carbon content in the catalyst layers. Furthermore, under some circumstances when electrode potentials are raised extremely high, there is a rapid degradation of carbon supports as well as of platinum.

4.2 Carbon Corrosion in PEMFCs

Several recent studies of carbon corrosion in a membrane electrode assembly of a PEMFC system found the process to be much more complicated than in aqueous solutions. The corrosion rate depends, among other factors, on the type of carbon, operating potential, temperature, humidity, and uniformity of fuel distribution. Generally, three types of carbon corrosion were identified (Fuller and Gray 2006).

The first one occurs under normal operating conditions. As (8) and (9) show, carbon is thermodynamically unstable owing to its low standard potential, which is much lower than the operating potential range of PEMFCs, and thus carbon corrosion can occur during the fuel operation at elevated temperatures. In practice, however, corrosion of conventional carbon supports, such as Vulcan, is insignificant at cell voltages lower than 0.8 V, but becomes a serious problem at voltages over 1.1 V (Roen et al. 2004). Furthermore, supported platinum nanoparticles catalyze carbon corrosion (Roen et al. 2004). Mathias et al. (2005) studied the kinetics of carbon corrosion as functions of temperature, potential, and time, estimating that 5 wt% of carbon (Ketjen black) would be lost over several thousand hours at open circuit voltage (0.9 V). Their study suggested that the stability of Ketjen black does not meet the requirements for automotive applications.

The second type of carbon corrosion in PEMFCs is elicited in the cathode by the partial coverage of hydrogen and oxygen in the anode. This phenomenon would be the most hazardous one in PEMFCs, especially for automotive applications wherein frequent start/stop cycling is expected. The mechanism of start/stop-induced carbon corrosion is as follows (Fig. 4) (Reiser et al. 2005; Stuve and Gastaiger 2006). During the start and shutdown of a cell, the anode would be partially covered by air from outside or from the cathode through the membrane. Thus, in an anode compartment, hydrogen oxidation reactions and ORRs can take place simultaneously.
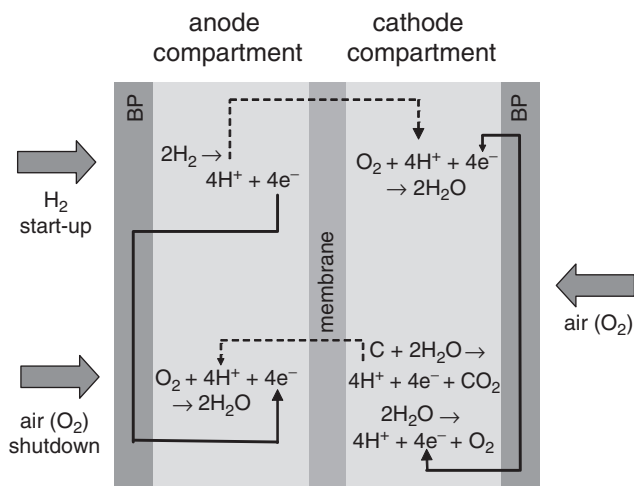
Fig. 4 Start/stop-induced carbon corrosion in the cathode (C + 2H$_2$O → 4H$^+$ + 4e^- + CO$_2$) when air is partially introduced in the anode (Reiser et al. 2005; Stuve et al. 2006). *Solid line*: electron path, *dashed line*: proton path

In a cathode compartment, the ORR and concomitant two anodic reactions, i.e., carbon dissolution (8) and oxygen evolution (2H$_2$O → 4H$^+$ + 4e^- + O$_2$), can occur at the same time. The flows of the electrons and the protons generated are designated by the solid line and the dashed line in Fig. 4, respectively. These reactions create a cathode interfacial potential difference of 1.44 V and higher in the hydrogen-starved region, triggering the evolution of oxygen and carbon corrosion on the cathode. We note that this "reverse-current" mechanism also exists during normal cell operation under localized fuel starvation even in a very small region, which likely happens simply by interrupting the fuel supply or blocking fuel in a single-flow channel (Satija et al. 2004; Fuller and Gray 2006; Patterson and Darling 2006). The very high potential generated by this mechanism, even for a short time, can severely damage the cathode by dissolving platinum and corroding carbon.

Fuel starvation causes the third mode of carbon corrosion that occurs on the anode (Reiser et al. 2005; Stuve et al. 2006). Supposing that no hydrogen is supplied to the anode but a cell potential of 0.7 V is maintained, then without hydrogen no anodic reaction at low potentials is feasible. Should the anode potential shift far above that of the cathode, then carbon dissolution and oxygen evolution reactions will occur on the anode.

High potentials may be loaded on the cathode and anode during the startup/ shutdown process and hydrogen starvation. Consequently, carbon supports and platinum degrade rapidly, thereby leading to significant loss in performance. To ensure the long-term life of PEMFCs, alternative supports have been considered, including carbon nanotubes (Shao et al. 2006, 2007; Wang et al. 2006a), oxides (Dieckmann and Langer 1998; Wu et al. 2005), carbides (Meng and Shen 2005; Nie et al. 2006), polymers (Lefebvre et al. 1999), boron-doped diamond (Wang and Swain 2002,

2003; Hupert et al. 2003; Fischer and Swain 2005; Fischer et al. 2007), and nonconductive whiskers (Parsonage and Debe 1994; Bonakdarpour et al. 2005; Debe et al. 2006). These materials have some advantages compared with carbon black, but also have issues and limitations hindering their applications as cathode supports in PEMFCs. Further information can be found in the recent review of Borup et al. (2007).

5 Stability of New Cathode Electrocatalysts

5.1 Platinum Monolayer on Metal Nanoparticle Electrocatalyst

Platinum monolayer electrocatalysts offer a dramatically reduced platinum content while affording considerable possibilities for enhancing their catalytic activity and stability. These electrocatalysts comprise a monolayer of platinum on carbon-supported metal or metal alloy nanoparticles. The platinum monolayer approach has several unique features, such as high platinum utilization and enhanced activity, making it very attractive for practical applications with their potential for resolving the problems of high platinum content and low efficiency apparent in conventional electrocatalysts (Adzic et al. 2007). Further, long-term tests of these novel electrocatalysts in fuel cells demonstrated their reasonably good stability. The synthesis of platinum monolayer electrocatalysts was facilitated by a new synthetic method, i.e., a monolayer deposition of platinum on a metal nanoparticle by the redox replacement of a copper monolayer (Brankovic et al. 2001). Three types of platinum monolayer electrocatalysts for the ORR were synthesized (1) platinum on carbon-supported palladium nanoparticles (Zhang et al. 2004), (2) mixed-metal platinum monolayers on palladium nanoparticles (Zhang et al. 2005a), and (3) platinum monolayers on noble/nonnoble core–shell nanoparticles (Zhang et al. 2005b). We discuss the results from the first option.

The experimentally measured electrocatalytic activity of platinum monolayers for the ORR shows a volcano-type dependence on the center of their d-bands, as determined by density functional theory (DFT) calculations (Zhang et al. 2005c). A monolayer of platinum on a palladium substrate was shown to have higher activity than the bulk platinum surface (Zhang et al. 2004), which partly reflects the decreased Pt–OH coverage in comparison with bulk platinum (PtOH, derived from H_2O oxidation on platinum, blocks the ORR). In addition, the small compression of a platinum deposit on a palladium substrate, causing a downshift of the d-band center, lowers the reactivity of platinum and slightly decreases platinum interaction with the intermediates in the ORR. Both effects enhance the ORR rates (vide infra) (Zhang et al. 2004, 2005a–c).

Long-term fuel cell tests were conducted using electrodes of $50\,cm^2$ with the Pt/Pd/C cathode catalyst containing $77\,\mu g\,cm^{-2}$ of platinum ($0.21\,g_{Pt}\,kW^{-1}$) and $373\,\mu g\,cm^{-2}$ of palladium. A commercial Pt/C electrocatalyst ($180\,\mu g\,cm^{-2}$ of platinum) was used for the anode. Figure 5a illustrates the trace of the cell voltage at a constant
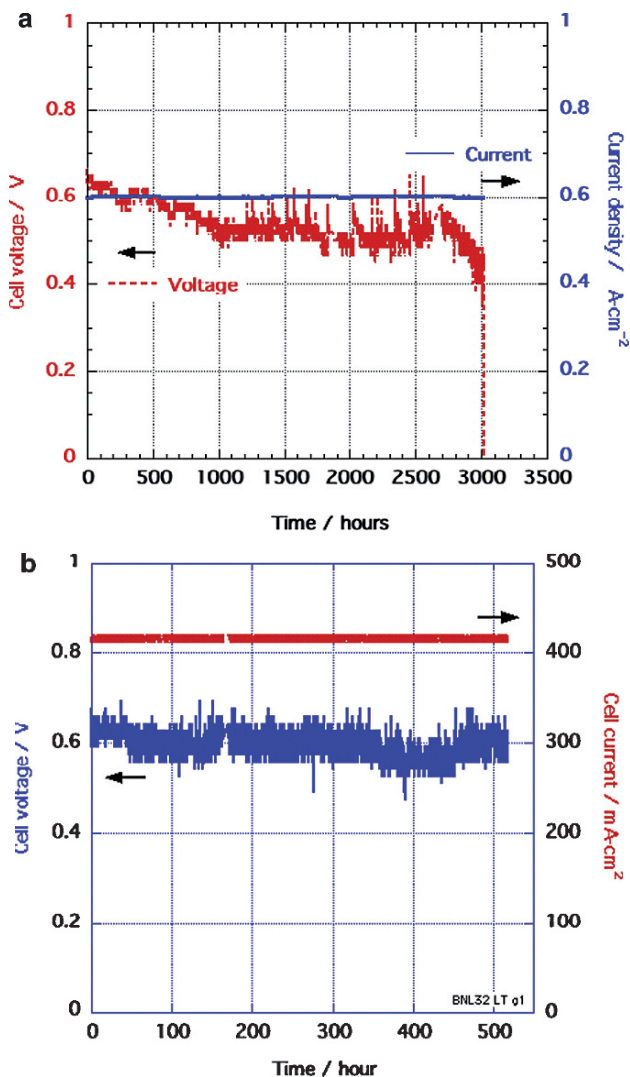
Fig. 5 The long-term stability tests of the Pt/Pd cathode electrocatalyst in an operating fuel cell at 80°C. (**a**) Commercial Pt/C anode catalyst. (**b**) Brookhaven National Laboratory's PtRu$_{20}$/C anode catalyst

current of 0.6 A cm^{-2} at 80°C against time. Up to 1,000 h, the cell voltage fell by about 120 mV, and then showed a much lower decrease with time. The total loss was approximately 140 mV by the end of the testing at 2,900 h. Compared with initial surface-area values, the losses of the platinum and palladium established by voltammetry were approximately 26% at 1,200 h and 29% at 2,000 h. The losses in platinum can be caused by dissolution of platinum at the operating potential or the embedment of platinum atoms into the palladium substrate; the latter mode is predicted

by a weak antisegregation of platinum on a palladium host according to DFT calculations (Greeley et al. 2002). We note that part of the observed drop in voltage also may be due to losses at the anode (a commercial Pt/C electrocatalyst) since the losses at the anode and cathode in these fuel cell measurements were not separated. The results are promising and improving further the electrocatalyst's long-time durability seems necessary.

Another long-term stability test was carried out using a fuel cell comprising both anode and cathode with platinum monolayer electrocatalysts of 5-cm^2 area (Fig. 5b). The cathode catalyst was Pt/Pd/C with platinum loading of 99 μg cm^{-2}, while the anode catalyst was Pt/Ru$_{20}$/C with platinum loading of 50 μg cm^{-2}. The latter, synthesized at Brookhaven National Laboratory by the electroless deposition of submonolayer platinum on ruthenium nanoparticles, exhibited enhanced activity for hydrogen oxidation, and had a low platinum loading (one-tenth of the standard loading) (Sasaki et al. 2004). When the cell was kept at a constant current density of 0.417 A cm^{-2}, it ran for 450 h with an average voltage of 0.602 V, with no significant loss of voltage. Its catalytic performance was 0.47 g$_{Pt}$ kW^{-1}. Membrane failure caused the termination of the test after 450 h of operation. Again, the results are promising, but further improvement is needed in the long-time durability of the electrocatalyst.

The stability of platinum monolayer electrocatalysts under conditions of potential cycling is higher than that of intrinsic platinum surfaces. We ascribed this advantage to a shift in the surface oxidation (PtOH formation) of monolayer catalysts to more positive potential than those for Pt/C. The shift is occasioned by the electronic effect of the underlying substrates, as discussed next.

5.2   Stabilization of Platinum Electrocatalysts Using Gold Clusters

The loss of platinum surface area in the cathode caused by the dissolution of platinum under the electrode potential cycling remains a serious obstacle for a widespread application of PEMFCs. In a recent report, Zhang et al. (2007b) demonstrated that platinum oxygen reduction electrocatalysts can be stabilized (exhibit negligible dissolution under potential cycling regimes) when platinum nanoparticles are modified with small gold clusters. Such increased stability was observed under the oxidizing conditions of the ORR and potential cycling between 0.6 and 1.1 V in 30,000 cycles. There were insignificant changes in the activity and the surface area of gold-modified platinum, in contrast to sizeable losses observed with platinum only under the same conditions. Also, these data offered the first evidence that small gold clusters can affect the properties of metal supports. The gold clusters were deposited on a Pt/C catalyst by the galvanic displacement by gold of a copper monolayer on platinum. The stabilizing effect of gold clusters on platinum was determined in an accelerated stability test by continuously applying linear potential sweeps from 0.6 to 1.1 V that cause the surface oxidation/reduction cycles of platinum.
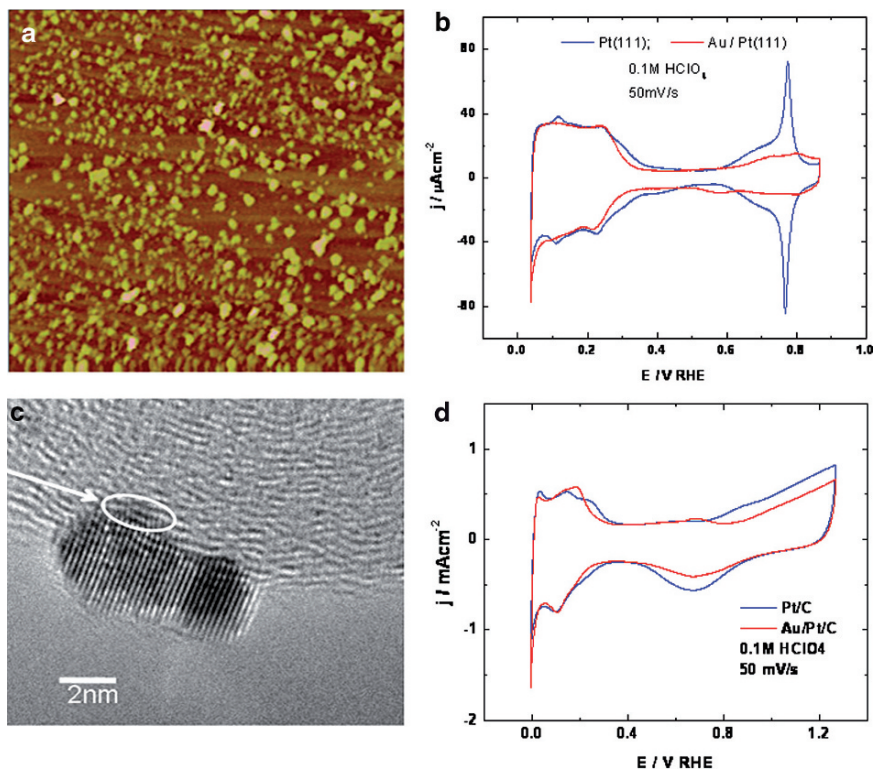
Fig. 6 (**a**) Scanning tunneling microscope image of gold clusters (two-thirds monolayer equivalent charge) and (**b**) the corresponding voltammetry curves for Pt(111) and Au/Pt(111). (**c**) Transmission electron microscope image of a gold-modified platinum nanoparticle and (**d**) the corresponding voltammetry curves

Figure 6a shows a scanning tunneling microscope image of gold clusters (two-thirds monolayer equivalent charge) and the corresponding voltammetry curves are shown in Fig. 6b, revealing that the gold clusters inhibit PtOH formation. Figure 6c displays a transmission electron microscope image of gold-modified platinum nanoparticles and the corresponding voltammetry curves are shown in Fig. 6d, revealing the same effect of gold as in Fig. 6b.

Figure 7 compares the catalytic activities of Au/Pt/C and Pt/C measured as the currents of O_2 reduction obtained before and after 30,000 potential cycles at the rate of $50\,mV\,s^{-1}$ of a thin-layer rotating disk electrode in an O_2-saturated $0.1\,M\,HClO_4$ solution at room temperature. There is only 5-mV degradation in the half-wave potential for Au/Pt/C after this period of potential cycling (Fig. 7a). The platinum surface area of the Au/Pt/C and Pt/C electrodes was determined by measuring hydrogen adsorption before and after potential cycling (Fig. 7b). Integrating the charge between 0 and $0.36\,V$ associated with hydrogen adsorption for Au/Pt/C revealed no difference, indicating that there was no recordable loss of the platinum
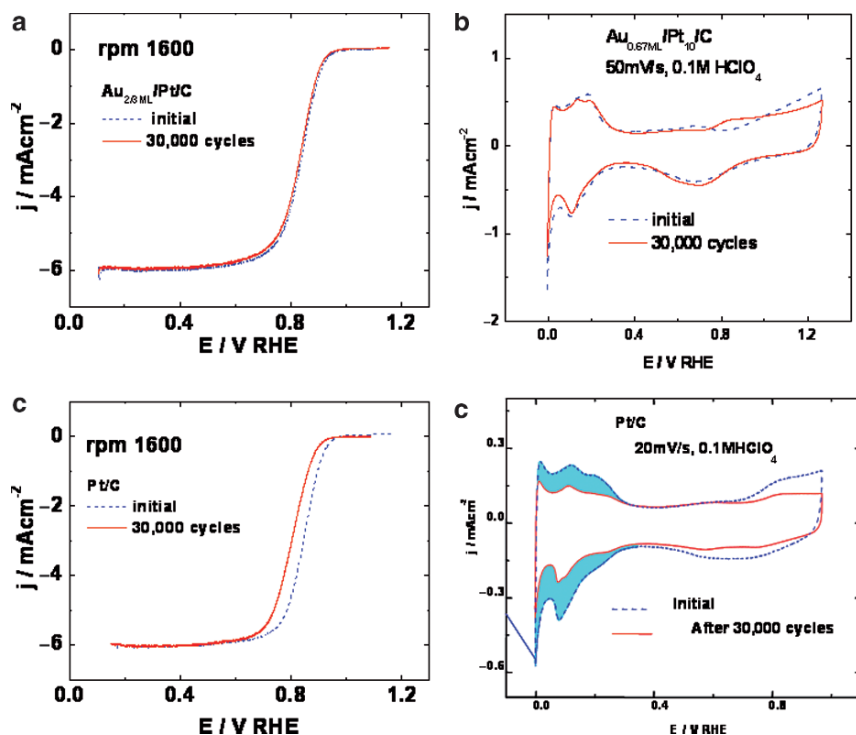
Fig. 7 Catalytic activities of Au/Pt/C and Pt/C measured as the currents of O$_2$ reduction obtained before (**a**) and after (**c**) 30,000 potential cycles from 0.6 to 1.1 V at the rate of 50 mV s^{-1} of a thin-layer rotating disk electrode in an O$_2$-saturated 0.1 M HClO$_4$ solution at room temperature. Corresponding voltammetry curves for the Au/Pt/C and Pt/C electrodes before (**b**) and after (**d**) potential cycling

surface area. However, for Pt/C, only about 55% of platinum surface area remained after such potential cycling (Fig. 7d), while the corresponding change in activity for Pt/C amounts to a loss of 39 mV (Fig. 7c). The same experiment with Au/Pt/C at 60°C showed no loss in activity, giving us additional evidence for the stabilization effect of gold clusters on the platinum support.

On the basis of an in situ X-ray absorption near-edge structure measurement, which explored the oxidation state of platinum as a function of potential for the Au/Pt/C and Pt/C surfaces, the origin of the observed stabilization effect of gold clusters was ascribed to a shifting of the oxidation of gold-covered platinum nanoparticles to more positive potentials than those without gold clusters (not shown). Another possibility for explaining the effect of gold clusters involves gold atoms diffusing to the kink- and step-platinum sites and blocking their interaction with the solution phase, consequently decreasing the platinum dissolution rate. The requisite mobility of gold on various surfaces has often been verified (Roudgar and Groβ 2004).

We can infer the electronic effects from theoretical work. Roudgar and Groβ (2004) used DFT calculations to demonstrate the coupling of d-orbitals of small

palladium clusters to the Au(111) substrate. An equivalent type of interaction between gold and platinum can account for the observed stabilization of platinum that, hence, can became "more noble" in its interactions with gold. Since clusters of a softer metal, gold, are placed on the surface of one that is considerably harder, platinum, there is practically no mixing between them; Del Popolo et al. (2005) earlier reached a similar conclusion about palladium on an gold system. The surface alloying of gold with platinum, although unlikely, also would modulate the electronic structure of platinum toward a lower surface energy, or lower-lying platinum *d*-band states. Thus, the interaction of gold clusters with metal surfaces differs from their interactions with the oxide supports. These findings hold promise for resolving the problem of platinum dissolution under potential cycling regimes, a feature that is critical for using fuel cells in electric vehicles.

6   Concluding Remarks

In this brief review of the dissolution and solubility of platinum under equilibrium conditions and the degradation of platinum nanoparticles at the cathode under various operating conditions, we discussed some mechanisms of degradation, and then offered recent possibilities for overcoming the problem. The data indicate that platinum nanoparticle electrocatalysts at the cathode are unstable under harsh operating conditions, and, as yet, often would be unsatisfactory for usage as the cathode material for fuel cells. Carbon corrosion, particularly under start/stop circumstances in automobiles, also entails electrical isolation and aggregation of platinum nanoparticles. We also discussed new approaches to alleviate the problem of stability of cathode electrocatalysts. One involves a class of platinum monolayer electrocatalysts that, with adequate support and surface segregation, demonstrated enhanced catalytic activity and good stability in a long-term durability test. The other approach rests on the stabilization effects of gold clusters. This effect is likely to be applicable to various platinum- and platinum-alloy-based electrocatalysts, causing their improved stability against platinum dissolution under potential cycling regimes. Such electrocatalysts, if supported on carbon with high corrosion stability (various graphitized carbons, carbon nanotubes, some oxides), look promising for resolving both stability problems so that fuel cells can be used in transportation in the near future.

References

Adzic, R. R., Zhang, J., Sasaki, K., Vukmirovic, M. B., Shao, M., Wang, J. X., Nilekar, A. U., Mavrikakis, M., Valerio, J. A. and Uribe, F. (2007) Platinum monolayer fuel cell electrocatalysts, Top. Catal. 46, 249–262.

Angerstein-Kozlowska, H., Conway, B. E. and Sharp, W. B. A. (1973) The real condition of electrochemially oxidized platinum surfaces, J. Electroanal. Chem. 43, 9–36.

Aragane, J., T. Murahashi and Odaka, T. (1988) Change of Pt distribution in the active components of phosphoric acid fuel cell, J. Electrochem. Soc. 135, 844–850.

Azaroual, M., Romand, B., Freyssinet, P. and Disnar, J.-R. (2001) Solubility of platinum in aqueous solutions at 25°C and pHs 4 to 10 under oxidizing conditions, Geochim. Cosmochim. Acta 65, 4453–4466.

Bett, J. A. S., Kinoshita, K. and Stonehart, P. (1976) Crystallite growth of platinum dispersed on graphitized carbon black: II. Effect of liquid environment, J. Catal. 41, 124–133.

Bi, W., Gray, G. E. and Fuller, T. F. (2007) PEM fuel cell Pt/C dissolution and deposition in nafion electrolyte, Electrochem. Solid-State Lett. 10, B101–B104.

Bindra, P., Clouser, S. J. and Yeager, E. (1979) Platinum dissolution in concentrated phosphoric-acid, J. Electrochem. Soc. 126, 1631–1632.

Birss, V. I., M. Chang and J. Segal (1993) Platinum oxide film formation-reduction: an in-situ mass measurement study, J. Electroanal. Chem. 355, 181–191.

Blurton, K. F., Kunz, H. R. and Rutt, D. R. (1978) Surface area loss of platinum supported on graphite, Electrochim. Acta 23, 183–190.

Bonakdarpour, A., Wenzel, J., Stevens, D. A., Sheng, S., Monchesky, T. L., Lobel, R., Atanasoski, R. T., Schmoeckel, A. K., Vernstrom, G. D., Debe, M. K. and Dahn, J. R. (2005) Studies of transition metal dissolution from combinatorially sputtered, nanostructured $Pt_{1-x}M_x$ (M = Fe, Ni; $0 < x < 1$) electrocatalysts for PEM fuel cells, J. Electrochem. Soc. 152, A61–A72.

Borup, R., Meyers, J., Pivovar, B., Kim, Y. S., Mukundan, R., Garland, N., Myers, D., Wilson, M., Garzon, F., Wood, D., Zelenay, P., More, K., Stroh, K., Zawodzinski, T., Boncella, J., McGrath, J. E., Inaba, M., Miyatake, K., Hori, M., Ota, K., Ogumi, Z., Miyata, S., Nishikata, A., Siroma, Z., Uchimoto, Y., Yasuda, K., Kimijima, K. I. and Iwashita, N. (2007) Scientific aspects of polymer electrolyte fuel cell durability and degradation, Chem. Rev. 107, 3904–3951.

Brankovic, S. R., Wang, J. X. and Adzic, R. R. (2001) Metal monolayer deposition by replacement of metal adlayers on electrode surfaces, Surf. Sci. 474, L173–L179.

Conway, B. E. (1995) Electrochemical oxide film formation at noble metals as a surface-chemical process, Prog. Surf. Sci. 49, 331–345.

Dam, V. A. T. and de Bruijn, F. A. (2007) The stability of PEMFC electrodes – platinum dissolution vs. potential and temperature investigated by quartz crystal microbalance, J. Electrochem. Soc. 154, B494–B499.

Darling, R. M. and Meyers, J. P. (2003) Kinetic model of platinum dissolution in PEMFCs, J. Electrochem. Soc. 150, A1523–A1527.

Darling, R. M. and Meyers, J. P. (2005) Mathematical model of platinum movement in PEM fuel cells, J. Electrochem. Soc. 152, A242–A247.

Debe, M. K., Schmoeckel, A. K., Vernstrorn, G. D. and Atanasoski, R. (2006) High voltage stability of nanostructured thin film catalysts for PEM fuel cells, J. Power Sources 161, 1002–1011.

Del Popolo, M. G., Leiva, E. P. M., Mariscal, M. and Schmickler, W. (2005) On the generation of metal clusters with the electrochemical scanning tunneling microscope, Surf. Sci. 597, 133–155.

Dieckmann, G. R. and Langer, S. H. (1998) Comparison of Ebonex and graphite supports for platinum and nickel electrocatalysts, Electrochim. Acta 44, 437–444.

Ferreira, P. J. and Shao-Horn, Y. (2007) Formation mechanism of Pt single-crystal nanoparticles in proton exchange membrane fuel cells, Electrochem. Solid-State Lett. 10, B60–B63.

Ferreira, P. J., la O', G. J., Shao-Horn, Y., Morgan, D., Makharia, R., Kocha, S. and Gasteiger, H. A. (2005) Instability of Pt/C electrocatalysts in proton exchange membrane fuel cells – a mechanistic investigation, J. Electrochem. Soc. 152, A2256–A2271.

Fischer, A. E. and Swain, G. M. (2005) Preparation and characterization of boron-doped diamond powder – a possible dimensionally stable electrocatalyst support material, J. Electrochem. Soc. 152, B369–B375.

Fischer, A. E., Lowe, M. A. and Swain, G. M. (2007) Preparation and electrochemical characterization of carbon paper modified with a layer of boron-doped nanocrystalline diamond, J. Electrochem. Soc. 154, K61–K67.

Fuller, T. F. and Gray, G. (2006) Carbon corrosion induced by partial hydrogen coverage, ECS Trans. 1, 345.

Garzon, F. H., Davey, J. and Borup, R. (2006) Fuel cell catalyst particle size growth characterized by X-ray scattering methods, ECS Trans. 1, 153.

Greeley, J., Norskov, J. K. and Mavrikakis, M. (2002) Electronic structure and catalysis on metal surfaces, Annu. Rev. Phys. Chem. 53, 319–348.

Gruver, G. A., Pascoe, R. F. and Kunz, H. R. (1980) Surface area loss of platinum supported on carbon in phosphoric acid electrolyte, J. Electrochem. Soc. 127, 1219–1224.

Guilminot, E., Corcella, A., Charlot, F., Maillard, F. and Chatenet, M. (2007a) Detection of Pt^{z+} ions and Pt nanoparticles inside the membrane of a used PEMFC, J. Electrochem. Soc. 154, B96–B105.

Guilminot, E., Corcella, A., Chatenet, M., Maillard, F., Charlot, F., Berthome, G., Iojoiu, C., Sanchez, J. Y., Rossinot, E. and Claude, E. (2007b) Membrane and active layer degradation upon PEMFC steady-state operation, J. Electrochem. Soc. 154, B1106–B1114.

Harrington, D. A. (1997) Simulation of anodic Pt oxide growth, J. Electroanal. Chem. 420, 101–109.

Healy, J., Hayden, C., Xie, T., Olson, K., Waldo, R., Brundage, A., Gasteiger, H. and Abbott, J. (2005) Aspects of the chemical degradation of PFSA ionomers used in PEM fuel cells, Fuel Cells 5, 302–308.

Honji, A., Mori, T., Tamura, K. and Hishinuma, Y. (1988) Agglomeration of platinum particles supported on carbon in phosphoric acid, J. Electrochem. Soc. 135, 355–359.

Hupert, M., Muck, A., Wang, R., Stotter, J., Cvackova, Z., Haymond, S., Show, Y. and Swain, G. M. (2003) Conductive diamond thin-films in electrochemistry, Diamond Relat. Mater. 12, 1940–1949.

Jerkiewicz, G., Vatankhah, G., Lessard, J., Soriaga, M. P. and Park, Y. S. (2004) Surface-oxide growth at platinum electrodes in aqueous H_2SO_4 reexamination of its mechanism through combined cyclic-voltammetry, electrochemical quartz-crystal nanobalance, and Auger electron spectroscopy measurements, Electrochim. Acta 49, 1451–1459.

Johnson, D. C., Napp, D. T. and Bruckenstein, S. (1970) A ring-disk electrode study of the current/potential behaviour of platinum in 1.0 M sulphuric and 0.1 M perchloric acids, Electrochim. Acta 15, 1493–1509.

Kinoshita, K. (1988) *Carbon: Electrochemical and Physicochemical Properties*, Wiley, New York, NY.

Kinoshita, K., Lundquist, J. T. and Stonehart, P. (1973) Potential cycling effects on platinum electrocatalyst surfaces, J. Electroanal. Chem. 48, 157–166.

Komanicky, V., Chang, K. C., Menzel, A., Markovic, N. M., You, H., Wang, X. and Myers, D. (2006) Stability and dissolution of platinum surfaces in perchloric acid, J. Electrochem. Soc. 153, B446–B451.

Lefebvre, M. C., Qi, Z. G. and Pickup, P. G. (1999) Electronically conducting proton exchange polymers as catalyst supports for proton exchange membrane fuel cells – electrocatalysis of oxygen reduction, hydrogen oxidation, and methanol oxidation, J. Electrochem. Soc. 146, 2054–2058.

Mathias, M. F., Makharia, R., Gasteiger, H. A., Conley, J. J., Fuller, T. J., Gittleman, C. J., Kocha, S. S., Miller, D. P., Mittelsteadt, C. K., Xie, T., Yan, S. G. and Yu, P. T. (2005) Two fuel cell cars in every garage?, Interface 14, 24–35.

Meng, H. and Shen, P. K. (2005) The beneficial effect of the addition of tungsten carbides to Pt catalysts on the oxygen electroreduction, Chem. Commun. 35, 4408–4410.

Mitsushima, S., Kawahara, S., Ota, K.-I. and Kamiya, N. (2007a) Consumption rate of Pt under potential cycling, J. Electrochem. Soc. 154, B153–B158.

Mitsushima, S., Koizumi, Y., Ota, K. and Kamiya, N. (2007b) Solubility of platinum in acidic media (I) – in sulfuric acid, Electrochemistry 75, 155–158.

Nagy, Z. and You, H. (2002) Applications of surface X-ray scattering to electrochemistry problems, Electrochim. Acta 47, 3037–3055.

Nie, M., Shen, P. K., Wu, M., Wei, Z. D. and Meng, H. (2006) A study of oxygen reduction on improved Pt-WC/C electrocatalysts, J. Power Sources 162, 173–176.

Ota, K.-I., Nishigori, S. and Kamiya, N. (1988) Dissolution of platinum anodes in sulfuric acid solution, J. Electroanal. Chem. 257, 205–215.

Parsonage, E. E. and Debe, M. K., (1994), U.S. Patent 5,338,430.

Patterson, T. W. (2002) *AIChE Spring National Meeting*, New Orleans, LA, pp. 313–318.

Patterson, T. W. and Darling, R. M. (2006) Damage to the cathode catalyst of a PEM fuel cell caused by localized fuel starvation, Electrochem. Solid-State Lett. 9, A183–A185.

Pourbaix, M. (1974) *Atlas of Electrochemical Equilibria*, 2nd ed., NACE, Houston, TX.

Rand, D. A. J. and Woods, R. (1972) A study of the dissolution of platinum, palladium, rhodium and gold electrodes in 1 M sulphuric acid by cyclic voltammetry, J. Electroanal. Chem. 35, 209–218.

Reiser, C. A., Bregoli, L., Patterson, T. W., Yi, J. S., Yang, J. D., Perry, M. L. and Jarvi, T. D. (2005) A reverse-current decay mechanism for fuel cells, Electrochem. Solid-State Lett. 8, A273–A276.

Roen, L. M., Paik, C. H. and Jarvi, T. D. (2004) Electrocatalytic corrosion of carbon support in PEMFC cathodes, Electrochem. Solid-State Lett. 7, A19–A24.

Roudgar, A. and Groβ, A. (2004) Local reactivity of supported metal clusters: Pd$_n$ on Au(111), Surf. Sci. 559, L180–L186.

Sasaki, K., Wang, J. X., Balasubramanian, M., McBreen, J., Uribe, F. and Adzic, R. R. (2004) Ultralow platinum content fuel cell anode electrocatalyst with a long-term performance stability, Electrochim. Acta 49, 3873–3877.

Satija, R., Jacobson, D. L., Arif, M. and Werner, S. A. (2004) In situ neutron imaging technique for evaluation of water management systems in operating PEM fuel cells, J. Power Sources, 129, 238–245.

Shao, Y., Yin, G., Zhang, J. and Gao, Y. (2006) Comparative investigation of the resistance to electrochemical oxidation of carbon black and carbon nanotubes in aqueous sulfuric acid solution, Electrochim. Acta 51, 5853.

Shao, Y., Yin, G. and Gao, Y. (2007) Understanding and approaches for the durability issues of Pt-based catalysts for PEM fuel cell, J. Power Sources 171, 558–566.

Shao-Horn, Y., Sheng, W. C., Chen, S., Ferreria, P. J., Hollby, E. F. and Morgan, D. (2007) Instability of supported platinum nanoparticles in low-temperature fuel cells, Top. Catal. 46, 285–305.

Stevens, D. A., Hicks, M. T., Haugen, G. M. and Dahn, J. R. (2005) Ex situ and in situ stability studies of PEMFC catalysts, J. Electrochem. Soc. 152, A2309–A2315.

Stuve, E. M. and Gastaiger, H. A., (2006), PEMFC short course, 210th Meeting of The Electrochemical Society, Cancun, Mexico.

Teranishi, K., Kawata, K., Tsushima, S. and Hirai, S. (2006) Degradation mechanism of PEMFC under open circuit operation, Electrochem. Solid-State Lett. 9, A475–A477.

Tseung, A. C. C. and Dhara, S. C. (1975) Loss of surface area by platinum and supported platinum black electrocatalyst, Electrochim. Acta 20, 681–683.

Virkar, A. V. and Zhou, Y. K. (2007) Mechanism of catalyst degradation in proton exchange membrane fuel cells, J. Electrochem. Soc. 154, B540–B546.

Voorhees, P. W. (1985) The theory of Ostwald ripening, J. Stat. Phys. 38, 231–252.

Wang, J. and Swain, G. M. (2002) Dimensionally stable Pt/diamond composite electrodes in concentrated H3PO4 at high temperature, Electrochem. Solid-State Lett. 5, E4–E7.

Wang, J. and Swain, G. M. (2003) Fabrication and evaluation of platinum/diamond composite electrodes for electrocatalysis – Preliminary studies of the oxygen-reduction reaction, J. Electrochem. Soc. 150, E24–E32.

Wang, X., Li, W. Z., Chen, Z. W., Waje, M. and Yan, Y. S. (2006a) Durability investigation of carbon nanotube as catalyst support for proton exchange membrane fuel cell, J. Power Sources 158, 154–159.

Wang, X. P., Kumar, R. and Myers, D. J. (2006b) Effect of voltage on platinum dissolution relevance to polymer electrolyte fuel cells, Electrochem. Solid-State Lett. 9, A225–A227.

Wilson, M. S., Garzon, F. H., Sickafus, K. E. and Gottesfeld, S. (1993) Surface area loss of supported platinum in polymer electrolyte fuel cells, J. Electrochem. Soc. 140, 2872–2877.

Wu, G., Li, L., Li, J. H. and Xu, B. Q. (2005) Polyaniline-carbon composite films as supports of Pt and PtRu particles for methanol electrooxidation, Carbon 43, 2579–2587.

Xie, J., Wood, D. L., More, K. L., Atanassov, P. and Borup, R. L. (2005a) Microstructural changes of membrane electrode assemblies during PEFC durability testing at high humidity conditions, J. Electrochem. Soc. 152, A1011–A1020.

Xie, J., Wood, D. L., Wayne, D. M., Zawodzinski, T. A., Atanassov, P. and Borup, R. L. (2005b) Durability of PEFCs at high humidity conditions, J. Electrochem. Soc. 152, A104–A113.

Yasuda, K., Taniguchi, A., Akita, T., Ioroi, T. and Siroma, Z. (2006a) Characteristics of a platinum black catalyst layer with regard to platinum dissolution phenomena in a membrane electrode assembly, J. Electrochem. Soc. 153, A1599–A1603.

Yasuda, K., Taniguchi, A., Akita, T., Ioroi, T. and Siroma, Z. (2006b) Platinum dissolution and deposition in the polymer electrolyte membrane of a PEM fuel cell as studied by potential cycling, Phys. Chem. Chem. Phys. 8, 746–752.

You, H., Chu, Y. S., Lister, T. E., Nagy, Z., Ankudiniv, A. L. and Rehr, J. J. (2000) Resonance X-ray scattering from Pt(1 1 1) surfaces under water, Physica B 283, 212–216.

Zhang, J., Mo, Y., Vukmirovic, M. B., Klie, R., Sasaki, K. and Adzic, R. R. (2004) Platinum monolayer electrocatalysts for O_2 reduction: Pt monolayer on Pd(111) and on carbon-supported Pd nanoparticles, J. Phys. Chem. B 108, 10955–10964.

Zhang, J. L., Vukmirovic, M. B., Sasaki, K., Nilekar, A. U., Mavrikakis, M. and Adzic, R. R. (2005a) Mixed-metal Pt monolayer electrocatalysts for enhanced oxygen reduction kinetics, J. Am. Chem. Soc. 127, 12480–12481.

Zhang, J., Lima, F. H. B., Shao, M. H., Sasaki, K., Wang, J. X., Hanson, J. and Adzic, R. R. (2005b) Platinum monolayer on nonnoble metal-noble metal core-shell nanoparticle electrocatalysts for O_2 reduction, J. Phys. Chem. B 109, 22701–22704.

Zhang, J. L., Vukmirovic, M. B., Xu, Y., Mavrikakis, M. and Adzic, R. R. (2005c) Controlling the catalytic activity of platinum-monolayer electrocatalysts for oxygen reduction with different substrates, Angew. Chem. Int. Ed. 44, 2132–2135.

Zhang, J., Litteer, B. A., Gu, W., Liu, H. and Gasteiger, H. A. (2007a) Effect of hydrogen and oxygen partial pressure on Pt precipitation within the membrane of PEMFCs, J. Electrochem. Soc. 154, B1006–B1011.

Zhang, J., Sasaki, K., Sutter, E. and Adzic, R. R. (2007b) Stabilization of platinum oxygen reduction electrocatalysts using gold clusters, Science 315, 220–222.